The final publication is available at

https://doi.org/10.1080/00423114.2023.2190031

Additional Information

Hardware-in-the-Loop simulations of a railway pantograph with a finite element periodic catenary model

J. Gil[a], M. Tur[a], S. Gregori[a,*], A. Correcher[b], A.M. Pedrosa[a], F.J. Fuenmayor[a]

[a]*Instituto de Ingeniería Mecánica y Biomecánica, Universitat Politècnica de València, Camino de Vera s/n, 46022, Valencia (Spain)*
[b]*Instituto de Automática e Informática Industrial, Universitat Politècnica de València, Camino de Vera s/n, 46022, Valencia (Spain)*

Abstract

The pantograph-catenary dynamic interaction problem is addressed by Hardware-in-the-Loop (HIL) tests to simulate the dynamic interaction between a numerical model (the catenary) and a physical device (the pantograph). The real-time simulation requires a computationally efficient numerical model and an on time and accurate transference of the response to the pantograph, for which a Periodic Finite Element Model (PFEM) of the catenary is considered. Firstly because of the acceptable computation time required to solve it, makes it suitable for real-time simulations and, secondly, its ability to allow for the delay caused by the transfer of the numerical model response.

The catenary PFEM we used considers the non-linear behaviour of the dropper slackening, leading to highly accurate HIL test results, which were validated up to a frequency of 25 Hz.

Keywords: Hardware-In-the-Loop, Hybrid Simulation, Pantograph, Control, Periodic Catenary

1. Introduction

The current research on railway engineering, is now involved in multiple problems, one of which is the pantograph-catenary dynamic interaction problem.

---

*Corresponding author

It is an established fact that, although there is still room for improvement, the performance of the pantograph-catenary couple limits the rolling stock speed. This is due to the apparent dynamic complexity of the system and the gap between the models and reality that hinders any attempt at improvement. This gap refers to the difficulty of reproducing experimental measurements by numerical simulations.

One of the solutions proposed to reduce the gap is the so-called Hardware-in-the-Loop (HIL) tests, also known as hybrid simulations (HS). These tests are used in multiple fields [1] and researchers have made great efforts to expand HIL boundaries. In the pantograph-catenary field, HIL tests consist of a pantograph loaded by an actuator that simulates the catenary response obtained from numerical simulations and can be considered midway between in-line experimental tests and pure numerical simulations.

Even though the use of HIL simulations is an appealing approach to avoid expensive in-line tests, their implementation presents certain challenges. HIL tests require very efficient models, advanced equipment and demanding electronic performance. One of the main requirements of HIL pantograph tests is thus a low computational cost of the catenary model as it needs to be integrated at a rate of 2 ms or less, which is high, considering the many degrees of freedom requiered of a catenary model to obtain accurate results. Another essential requirement is a short control loop delay to prevent an unstable response. To solve these two big problems, different efficient catenary models and techniques to mitigate the effect of the delay can be found in the literature.

The modal-truncated approach is used in [2, 3] to reduce the size of simplified catenary models as regards the computational cost. The same approach is also used in [4] but applied to a non-linear finite element catenary model. Another alternative is the sliding window method, which was first used in [5] with a simple catenary model composed of three spans. This model was upgraded in [6] by the inclusion of non-linear dropper slackening behaviour. In [7] a catenary model based on a moving mesh formulation in combination with absorbing boundary layers was used to perform catenary time integration in real-time. All

2

these finite-length catenary models lead to a stationary response that is affected by the boundary conditions assumed.

Although the previously described catenary models can be computed in real-time, their response has to be faithfully transferred to the physical device, and the presence of a delay prevents this. Some solutions have been proposed to address the negative effects of delays. In [8], the HIL technique is applied to the vehicle-bridge interaction and the work aims to compensate the HIL delay by using a recursive prediction optimal (RPO) compensator. This method has been shown to have better performance than other strategies such as polynomial extrapolation [9], inverse compensation [10] or differential feedforward [11]. The interaction between a real pantograph and a virtual catenary is dealt with in [12, 13]. This type of simulation is called a Dynamically Substructured System (DSS) as the interaction is conducted in a different way to that used in HIL. According to the authors, the HIL or HS labels are used when the interaction between the virtual and psysical substructure follows an open-loop strategy. In the HIL strategy, transferring the response of the virtual to the physical model therefore has to be ideal, implying rigorous requirements. On the other hand, DSS provides an interaction between the models by means of a closed loop in which the response of the virtual model is compared to the current status of the physical device and a control action is included. In [12], the control system is developed via Linear Sub-structuring Control (LSC) to perform DSS by a very elementary catenary model with one degree of freedom and variable stiffness. Experimental results can be achieved by replacing the pantograph with a shock absorber, which is good for the control field but is still far from accurate in representing the pantograph-catenary dynamic interaction. This approach was continued in [13] by applying a sliding window approach to model the catenary, but the test was performed with the same simplified pantograph model. The results obtained were compared with simulations but were seen to be significantly inaccurate. In [14], the DSS strategy was then tested with a real pantograph and the accuracy of the results was challenged. According to this terminology, the work conducted in [7] could be described as DSS, since they

3

also developed a control algorithm based on the energy equation to limit the error in the controlled position of the catenary to avoid the instability produced by delays.

In the present work we adopted the periodic finite element model of the catenary proposed in [15]. This model provides highly accurate results, as demonstrated in [15], accounts for dropper slackening and has certain advantages for its practical implementation. Due to the infinite periodicity foundation, the steady-state solution provided by the PFEM is not influenced by the boundary-layer effects. The model is also suitable for a total delay compensation technique, which has shown good performance in virtual tests [15]. Our main aim was thus to describe the most important factors to be taken into account in performing HIL pantograph tests with the above-cited catenary PFEM. We also describe in detail the iterative algorithm used to achieve the steady-state regime and practical measures to prevent test instability. The HIL test results were validated by a proposed method that can quantify the overall HIL-induced error.

The remainder of this paper is organised as follows: Section 2 gives a description of the test rig used in the HIL tests. Section 3 describes the two strategies used to perform HIL tests with the PFEM. Section 4 performs a stability parametric analysis of the two strategies proposed. Section 5 validates the HIL setup and presents some of the results of different catenaries and train speeds, while Section 6 sums up our main conclusions.

2. HIL test-rig

The test rig used for the real-time interaction of virtual catenaries and real pantographs is shown in Fig. 1. Its main elements are as follows:

4
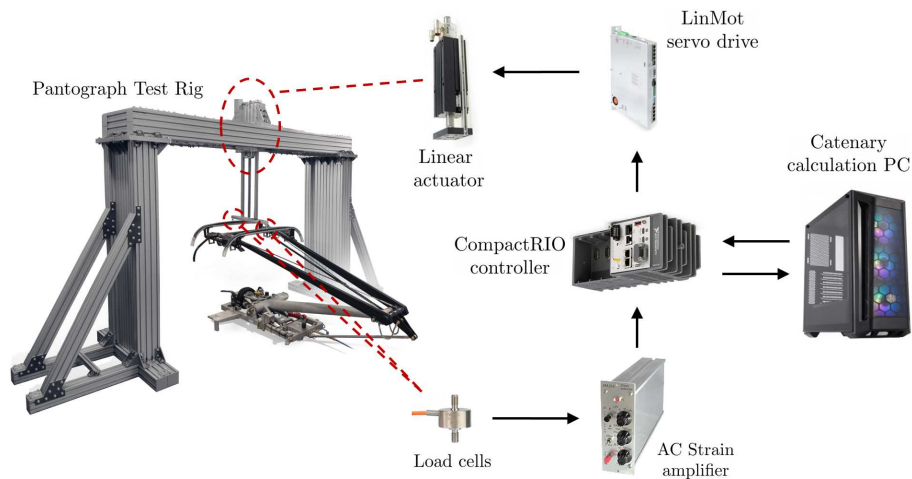
Figure 1: *Test-rig components and information flow.*

- **Actuator:** A linear magnetic motor (LINMOT PS10-70x240U) with a maximum velocity of 5.4 m/s and a maximum force of 1650 N.

- **Actuator Controller:** The E1450 motor drive controller receives position references by UDP communication via a LinUDP bespoke protocol. The controller generates intermediate sub-references using one of the several sub-reference generation modes. The selected working mode is a linear interpolation (ramp) between reference points to avoid generating parasite frequencies and discrete steps that lead to instability. A closed-loop PID control strategy is used to follow all the sub-references generated. Since communications with the driver are non-deterministic, the sub-references are executed by a hardware trigger signal generated by the Real-Time Computer to guarantee periodic execution of the control commands.

- **Real-Time Computer:** A real-time *CompactRio* (CRIo-9040) device from National Instruments™ forms the system's brain, which carries out the main tasks. It includes a Dual Core 1.30 GHz processor, 2GB RAM, Ethernet communications, and several IO modules. The RT computer acquires the measured force. It also executes the main and control loops.

The main loop has a rate of 2 ms in which it adquires the force value, sends the value to the computer and receives its response. The motor control loop has a rate of 10 ms in which it acquires the last displacement value of the main loop and sends it to the Actuator Controller.

- **PC:** This solves the virtual catenary PFEM implemented in Matlab™. As it is essential to have a flexible code to test different settings of the catenary in different experiments, this code runs on an Intel®Core™ i9, 3.6GHz, eight cores and 64Gb RAM PC high-speed processor.

- **Force measuring:** Two load cells measure the force of the pantograph on the actuator. These signals are conditioned by two AC Strain amplifiers (AS1201) that increase the signal levels and include a configurable filtering stage (10Hz, 30Hz, 100Hz, 300Hz, or no filter).

- **Pantograph:** The pantograph selected for this research is a DSA®380.03.

The test rig materialises the vertical displacement of the catenary contact point when a force is applied. The process carried out, since this force is measured until the actuator achieves the response given by the catenary model, follows the itinerary defined in Fig. 2. The time that this process takes has a great influence on the accuracy of the response. The process starts when the force is measured, then passes through a filter and the signal is converted into a digital value by the AD converter. The force value is picked by the RT computer at the beginning of the RT main loop. The following step in this main loop is to send the force to the PC, which after solving one time step of the catenary dynamics, answers with the displacement value of the catenary that is waiting to be sent at the beginning of the control loop. As the value is received by the motor driver that controls the actuator, the driver imposes intermediate values following a ramp between the former and the current references. The ramp finishes on receiving a new reference.

The different parts that account for the total delay can be identified by following the above-described path. The acquisition keeps getting values very

6

quickly until the Main Loop of the RT computer picks one (negligible delay). 2 ms are spent until the iteration of the Main Loop is finished and the value enters the Control Loop. The force value is sent to the actuator controller, taking approximately 4 ms, and at this point a ramp of 10 ms (the time necessary to get the next reference) starts. The total delay is thus 16 ms.
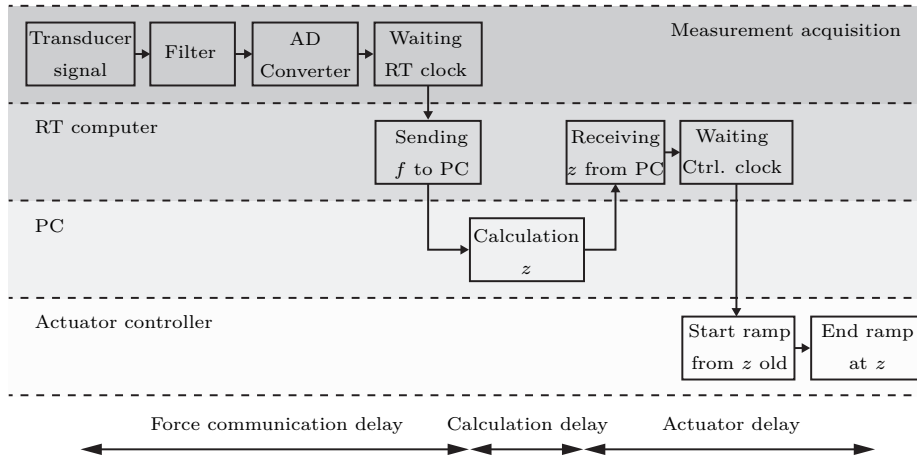
Figure 2: *Itinerary of the whole loop of the test rig*

3. Iterative algorithm of the HIL pantograph tests

The catenary model used for the pantograph-catenary HIL test consists of a periodic catenary modelled by the finite element method, which considers non-linear dropper slackening behaviour. This model reproduces the steady-state dynamic solution of the catenary under the action of a load moving at constant speed, which is representative of the central catenary spans of the pantograph-catenary interaction.

The method used aims to find the steady-state solution of the pantograph-catenary coupled system by means of the HIL rationale, in which the physical device (pantograph) and the virtual model (catenary) of both systems are coupled (the pantograph is governed by transient dynamics and the virtual model satisfies the steady-state equilibrium). To reach this stationary regime it is nec-

7

essary to use an iterative procedure to traverse the inevitable transient period. Both the catenary model and the iterative strategy used to guide the HIL test were proposed in [15].

In this section, the linear version of the catenary model and the iterative algorithm are first briefly described, emphasising the main differences required to implement them in a test environment. A new variant of the iterative algorithm is also proposed to tackle the stability issues that arise in practical implementations, and the strategy used to consider dropper non-linear behaviour is also introduced.

3.1. HIL tests with a linear PFEM of the catenary

This section briefly introduces the key ideas of the framework proposed in [15], although for further information the reader is referred to [15], which provides the steady-state response of an infinite periodic catenary subjected to a moving load for a discrete-time environment. The solution relates the periodic moving load vector $\mathbf{f}$ with the contact wire vertical position $\mathbf{z}$ due to the application of this load vector. Due to the existing periodicity, the time domain includes only the time taken by the load to travel across one span of the catenary and is discretised into N steps, so that the time step $n, \hat{n} \in [1, ..., N]$, n being the time step of a given displacement and $\hat{n}$ the time step of the load-application point. Given a complete set of contact forces $f(\hat{n})$ arranged in vector $\mathbf{f}$, the contact wire height $\mathbf{z}$ vector, which includes the contact points $z(n)$, can be directly obtained as:

$$\mathbf{z} = \mathbf{z}_0 + \mathbf{I}_{\mathrm{cc}}\mathbf{f} \tag{1}$$

$\mathbf{z_0}$ being the initial configuration contact point height (initial geometric catenary shape). With this scheme, the vertical displacement of the contact point $u(n)$, for all the time steps within the span, can be calculated by means of the product of the contact force $\mathbf{f}$ and matrix $\mathbf{I}_{\mathrm{cc}}$ which contains the contribution of every load value (column index $\hat{n}$) to every displacement value (row index n).

The proposed model can give a response, provided the periodic contact force is known. This assumption does not apply to HIL tests, in which the force is

8

measured and is not periodic (at least at the beginning of the test). The strategy of accomplishing HIL tests with a catenary PFEM was proposed in [15]. Roughly speaking, the goal is to measure the contact force along a span, compute the catenary response and impose this vertical position with a periodic assumption, even if the contact force is not periodic, assuming that an iterative process will reach the steady state.

HIL tests are performed following a discrete time scheme. In each global time step, denoted by index k, every contact point displacement is imposed and its contact force is measured. This global time is also organised in blocks of N samples in the form of the length of a period in the problem. The time is denoted in every block b by index $\bar{n}$, starting from 1 at the beginning of the block. The measured contact force in a given time step is denoted as $\bar{f}(k)$ and the vertical position of the actuator in this time step as $\bar{z}(k)$, which depends on the contact force of the previous time steps, as will be explained below. When the test reaches convergence, displacement and forces are repeated in every block and must satisfy Eq. (1). The measured contact force can also be referred to as $\bar{f}^b(\bar{n})$ and the position sent to the actuator as $\bar{z}^b(\bar{n})$, since every global time step k represents a a local time step $\bar{n}$ in block b.

Two alternatives are proposed in this paper for the iterative protocol of the HIL test, i.e. step-by-step and span-by-span updating. In the former we need to compute the displacement of the next step in every time step in which the force is measured, while the span-by-span updating strategy initially defines the position of the actuator along the whole span.

3.2. Step-by-step updating

The method used to perform step-by-step HIL tests with the periodic catenary model is represented in the scheme in Fig. 3. Note that the global time of the test is represented by the markers on the horizontal line. The different points in the figure are as follows:

- Point 1: Let us say that the test is in the k global time step (or time step $\bar{n}$ within the block b, as represented by the pantograph illustration) and

9

the pantograph has reached the displacement sent from the previous time step $k-1$.

- Point 2: The force $\bar{f}^b(\bar{n})$ is measured simultaneously to Point 1.

- Point 3: The measured force is placed in vector $\mathbf{f}^k$ (which changes every time step k, as denoted by the superscript) in the right position $\bar{n}$ while the other elements of this vector remain unaltered.

- Point 4: Eq. (1) is applied to compute the response of the periodic model with $\mathbf{f}^k$, producing the $\mathbf{z}^k$ vector which replaces the one in the previous step $k-1$. Note that in this case, all the components in vector $\mathbf{z}^k$ change.

- Point 5: The vertical position of the next step $\bar{n}+1$ is taken from $\mathbf{z}^k$ since this is the position that would be reached in the next step $k+1$. At this point, a more advanced position to $\bar{n}+1$ can be extracted from $\mathbf{z}^k$ in order to compensate for any possible delay.

- Point 6: The displacement is sent to the actuator.

- Point 7: It is time to move to the next step and the timeline depicted at the bottom of the figure moves one position to the left, so that the pantograph can reach the position sent from point 6. The indexes of Points 3 and 5 drop down a position to be ready to receive and give the right values in the next step $k+1$.

In Point 4, the PFEM's response is computed according to Eq. (1), but as explained in [15], a mathematically equivalent formulation can be used to reduce the computation time. Then, $\mathbf{z}^k$ can be equivalently obtained by considering the force increment in every time step:

$$\mathbf{z}^k = \mathbf{z}^{k-1} + \mathbf{I}_{\text{cc}}(\bar{n})(\bar{f}^b(\bar{n}) - \bar{f}^{b-1}(\bar{n})) \tag{2}$$

due to the fact that only one element of vector $\mathbf{f}^k$ is changed in every time step.
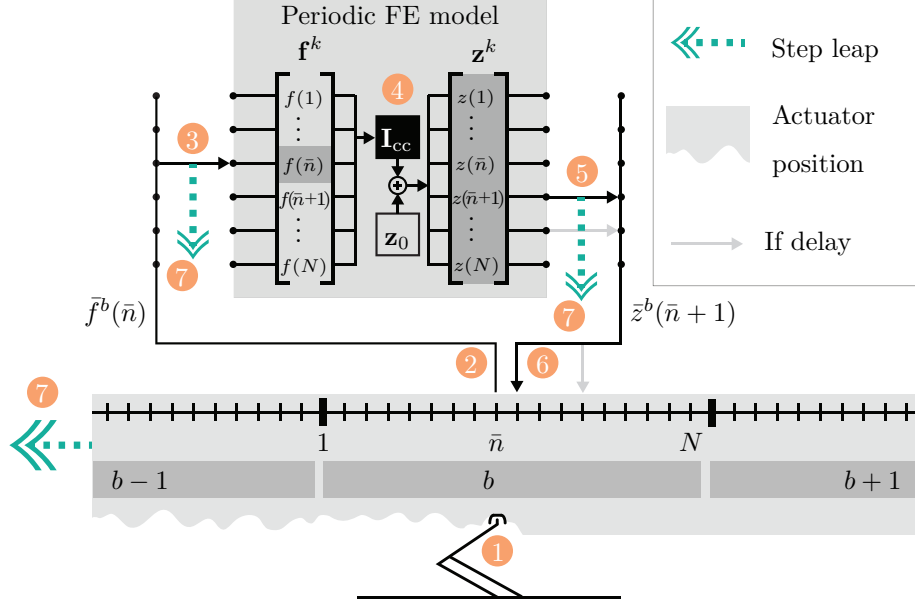
Figure 3: *Graphical description of the step-by-step HIL test architecture with a PFEM of the catenary.*

3.3. Span-by-span updating

A different updating strategy is here proposed to circumvent some convergence issues. This new strategy follows the four first points listed in Section 3.2 and shown in Fig. 3, but the differences arise in Point 5. Whereas a single value of vector $\mathbf{z}^k$ was extracted in the step-by-step strategy and it would continue its way to Point 6, in the span-by-span updating strategy there is a memory rack between Points 5 and 6. Only at the time step $\bar{n} = N$ (at the end of each block) the whole vector $\mathbf{z}^k$ is extracted and its N values are stored in the memory. The stored vector is called $\mathbf{z}^b$ and it fulfils $\mathbf{z}^b = \mathbf{z}^k$ if $k = bN$. According to the proposed scheme, the displacement $\bar{z}^b(\bar{n})$ sent to the actuator in Point 6 is computed from the stored vectors $\mathbf{z}^b$ of the two previous blocks, combining both with linear shape functions to avoid lack of continuity at the beginning of a new block, i.e.:

11

$$\bar{z}^b(\bar{n}) = N_1(\bar{n})z^{b-2}(\bar{n}) + N_2(\bar{n})z^{b-1}(\bar{n}) \ ; \quad \bar{n} \in [1, N] \qquad (3)$$

in which N_1 and N_2 are linear shape functions which go from 1 to 0 and from 0 to 1, respectively. This method has a different performance in terms of stability, which will be discussed in Section 4.

3.4. Delay compensation

As mentioned in Section 2, there is a consumed time in the test loop (see Fig. 2) that delays the response of the catenary. A delay of D time steps exists from the moment at which the contact force is measured in Point 2 (Fig. 3) until the pantograph reaches the position computed in Point 5. Fig. 3, represents the unavoidable delay of one step $D = 1$, but an extra delay is also considered in Point 6 of the figure by a grey arrow. If the position sent to the actuator takes the path defined by the grey arrow, it will be placed in a later position on the timeline because it will need more time steps to be achieved by the pantograph.

Note that this delay does not affect the rate of the loop, the pantograph will reach the sent position later but it does not prevent the next time step from starting. One of the main advantages of the catenary PFEM is that this delay can be easily allowed for because the contact wire height $\mathbf{z}^k$ includes the displacement values at all times n in the span. To compensate for a given delay, the position value extracted in Point 5 in Fig. 3 is thus the $n = \bar{n} + D$ indicated by the grey arrow. This procedure eliminates the error produced by the delay in the dynamic response, since at the end of the test, when convergence is achieved, $\mathbf{f}^k$ and $\mathbf{z}^k$ do not change and the value at time step $n = \bar{n} + D$ will be a perfect prediction.

3.5. Frequency content reduction

Another important aspect to consider is that we can limit the frequency content of the actuator displacement. As vector $\mathbf{z}$ is periodic, it can be shifted to the frequency domain by the discrete Fourier transform (DFT) and then the

12

higher frequencies can be removed before being brought back to the time domain by the inverse discrete Fourier transform (IDFT).

A number of N_{h} frequencies (the zeroth harmonic included) are considered in this frequency reduction, f_{max} being the highest frequency included. This number plays an important role in the stability of the HIL test because if f_{max} is higher than the biggest frequency that the gear can control it will lead to deficient performance. The whole process can be done directly by applying matrix operations to $\mathbf{z}$. Let us define the DFT matrix operator as:

$$\mathbf{W} = e^{\frac{-2\pi i}{N}\mathbf{mn}^{\top}} \qquad \text{for} \qquad \begin{aligned} \mathbf{m} &= [0, 1, ..., N_{\text{h}} - 1]^{\top} \\ \mathbf{n} &= [0, 1, ..., N - 1]^{\top} \end{aligned} \tag{4}$$

With the same approach, the IDFT matrix can be obtained as:

$$\mathbf{V} = \frac{1}{N} e^{\frac{2\pi i}{N}\mathbf{nm}^{\top}} \mathbf{A} \tag{5}$$

$\mathbf{A}$ being an $N_{\text{h}} \times N_{\text{h}}$ diagonal matrix with a 1 in the first element of the diagonal and a 2 in the other components, to duplicate the value of columns 2 to N_{h} of matrix $\mathbf{V}$ due to considering the unilateral representation of the DFT. These two operations defined in Eqs. (4) and (5) can be combined in a single matrix, i.e.:

$$\widetilde{\mathbf{W}} = \text{Re}(\mathbf{VW}) \tag{6}$$

Thus, to filter vector $\mathbf{z}$, Eq.(1) is multiplied by $\widetilde{\mathbf{W}}$:

$$\widetilde{\mathbf{z}} = \widetilde{\mathbf{W}}\left[\mathbf{z}_0 + \mathbf{I}_{\text{cc}}\mathbf{f}\right] \tag{7}$$

This filtering operation can be precomputed by applying the operator $\widetilde{\mathbf{W}}$ to $\mathbf{I}_{\text{cc}}$ and $\mathbf{z}_0$ so that Eq. (1) is rewritten as:

$$\widetilde{\mathbf{z}} = \widetilde{\mathbf{z}}_0 + \widetilde{\mathbf{I}}_{cc}\mathbf{f} \tag{8}$$

3.6. Relaxation coefficient and initial ramp

Another difference between the numerical algorithm proposed in [15] and that used to perform HIL tests relies on a relaxation coefficient μ_{c} to reduce

13

the sharp change between the response of successive blocks during the iterative procedure. In Point 3 in Fig. 3, the measured force replaces the element $\bar{n}$ of $\mathbf{f}^k$, in which the measure of the previous block was previously allocated. If the relaxation is applied, the current measurement will be relaxed with the old one, resulting in:

$$^{\mathrm{r}}\bar{f}^b(\bar{n}) = {}^{\mathrm{r}}\bar{f}^{b-1}(\bar{n}) + \mu_{\mathrm{c}}(\bar{f}^b(\bar{n}) - {}^{\mathrm{r}}\bar{f}^{b-1}(\bar{n})) \tag{9}$$

which will be allocated finally in the void. This relaxation can be included in Eq. (2)

$$\mathbf{z}^k = \mathbf{z}^{k-1} + \mu_{\mathrm{c}}\mathbf{I}_{\mathrm{cc}}(\bar{n})(\bar{f}^b(\bar{n}) - {}^{\mathrm{r}}\bar{f}^{b-1}(\bar{n})) \tag{10}$$

This coefficient is used to ensure convergence of the test and plays an important role in the stability of the iterative method, as explained in Section 4.

To avoid a sudden jump at the beginning of the HIL test, the height sent to the actuator is scaled by a factor that varies linearly from 0 to 1 step by step, thus defining an initial ramp that lasts N_r steps.

3.7. Considering dropper slackening

In Point 4 of the loop (see Fig. 3), Eq. (1) is used to compute the response of the catenary, given a contact force, although additional external actions can also be applied. Non-linear dropper slackening behaviour is essential to perform accurate simulations and can be considered by adding external correction forces, which depend on the elongation of the droppers, as explained in [15]. If matrix $\mathbf{I}_{\mathrm{c}d}$ includes the stationary response of the contact point produced by a compressive force acting on both ends of dropper d, then Eq. (1) can be extended to:

$$\mathbf{z} = \mathbf{z}_0 + \mathbf{I}_{\mathrm{cc}}\mathbf{f} + \sum_{d=1}^{N_{\mathrm{d}}} \mathbf{I}_{\mathrm{c}d}\mathbf{f}_d \tag{11}$$

in which $\mathbf{f}_d$ is the correction force vector of dropper d, N_{d} is the total number of droppers. Note that $\mathbf{I}_{\mathrm{c}d}$ rows indicate the time step of the contact point displacement and its columns are related to the time step of the dropper force application.

14

So far, the response of the catenary has been evaluated at the contact point only, but hereinafter the dropper elongation also needs to be computed. Let us define matrices $\mathbf{I}_{dc}$ and $\mathbf{I}_{dd}$, which account for the dropper elongation produced by the contact force and the other droppers' correction forces, respectively. The total elongation of dropper d can therefore be computed as:

$$\mathbf{\Delta L}_d = \mathbf{I}_{dc}\mathbf{f} + \sum_{d=1}^{N_\mathrm{d}} \mathbf{I}_{dd}\mathbf{f}_d \tag{12}$$

As in $\mathbf{z}$, it is important to limit the frequency content of $\mathbf{\Delta L}_d$ in order to ease the convergence of the method. To this end, the terms involved in Eq. (12) are pre-multiplied by the matrix $\widetilde{\mathbf{W}}_d$, which is built like $\widetilde{\mathbf{W}}$ (see Section 3.5), but considering in this case a different number of harmonics N_hd.

In the same way that $\mathbf{f}^k$ is treated in Point 4 of the HIL loop, vector $\mathbf{f}_d^k$ is modified in each time step $\bar{n}$ by replacing the corresponding elements with the dropper forces computed in that step. As described in Section 3.6, relaxation can also be applied to $\mathbf{f}_d^k$ with a coefficient μ_d (See [15] for further information).

4. Stability parametric analysis

This section describes the stability of the proposed method, which depends on several factors: the catenary model, the pantograph, the frequencies included in the catenary response, the stiffness of the contact, the relaxation coefficient and the delay. For the sake of simplicity, stability is studied in a computational environment, replacing the real pantograph by a numerical model and using the *penalty* method as the contact model and performing a numerical time integration in what we call a virtual HIL test.

To study the stability it is necessary to express the problem as a linear iterative process in which the variables or state vector in any iteration can be written as a linear operation applied to the previous state. In the specific problem of a virtual HIL test, the iterative formulation has a certain complexity because the concept of iteration refers to an entire block iteration instead of a

time-step iteration, so that every iteration includes the application of another iterative method to numerically integrate the dynamic response of the pantograph model.

The state vector of block b, $\mathbf{X}^b$, considers the necessary variables to compute the state vector of the next block, such as the displacement/force of the contact point in every time step, among others. This section mainly defines the iterative linear operation to analyse the stability of the method by means of the spectral radius, which can be written as:

$$\mathbf{X}^{b+1} = \mathbf{A}\mathbf{X}^b + \mathbf{B} \tag{13}$$

in which all the vectors and matrices depend on the HIL strategy followed (their definitions can be found in Appendix A). Once the matrices in Eq. (13) are obtained, the virtual HIL test can be conducted by applying this linear operation iteratively, and the stability of the iterative procedure can be determined by the spectral radius of matrix $\mathbf{A}$.

Parametric studies are performed for the span-by-span and step-by-step approaches to analyse the stability of the proposed HIL strategy, including the influences of the number of harmonics considered in the catenary response N_{h} (related to the higher frequency f_{max}), and the contact stiffness k_c. We use a specific stitched catenary model (defined in Section 5) and a one-degree-of-freedom pantograph model, also considering the delay in our actual test rig. The pantograph model has a mass of 6.6 kg, a stiffness of 7000 N/m and a damping of 10 Ns/m and similar behaviour to the pantograph used in real HIL tests. The frequency of the loop is $\Delta t = 2$ ms and the delay is $D = 8$.

The spectral radius obtained by the span-by-span updating strategy is shown in Fig. 4 (a) for different f_{max} and k_c. Values bigger than 1, that indicate unstable behaviour, are hidden in white. At every point on the map, the value of the relaxation coefficient μ_{c}, which minimises the spectral radius, is chosen and plotted in Fig. 4 (b). The same information is shown in Fig. 5 for the step-by-step updating strategy. The solid red curve highlights the natural frequency of

16

the pantograph model, including contact stiffness. The span-by-span approach

³⁷⁵ results can be seen to be more stable, and the pantograph's natural frequency
is a barrier to stability. Higher contact stiffness can therefore improve stability
and it is required to reduce the number of frequencies involved in the response
of the catenary model below the natural frequency related to the pantograph
contact degree of freedom.

(a) *Spectral radius* **(b)** μ_c *optima*
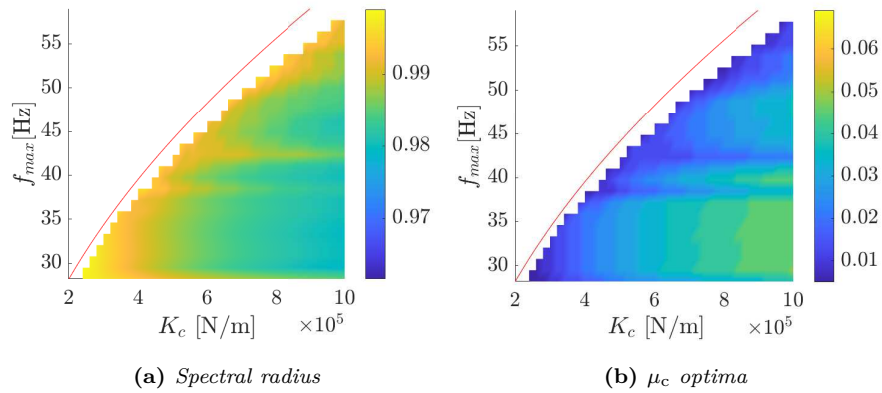
Figure 4: *Stability analysis of the span-by-span updating scheme with delay $D = 8$.*

(a) *Spectral radius* **(b)** μ_c *optima*
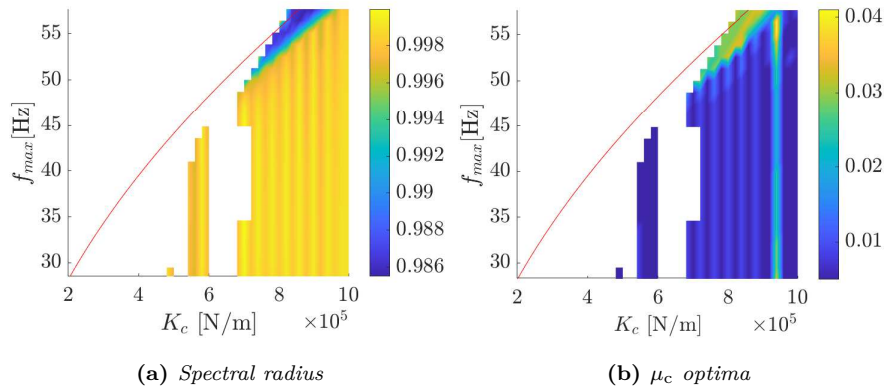
Figure 5: *Stability analysis of the step-by-step updating scheme with delay $D = 8$.*

³⁸⁰ Unlike the span-by-span method, the delay plays a fundamental role in sta-
bility in the step-by-step strategy. Fig. 6 shows a similar representation but

17

with a contact stiffness $k_c = 6 \cdot 10^5$ N/m and including the delay as a parameter. The figure shows a repetitive pattern of the delay, which makes possible including an additional delay to achieve a stable zone.


(a) *Spectral radius*

(b) μ_c *optima*
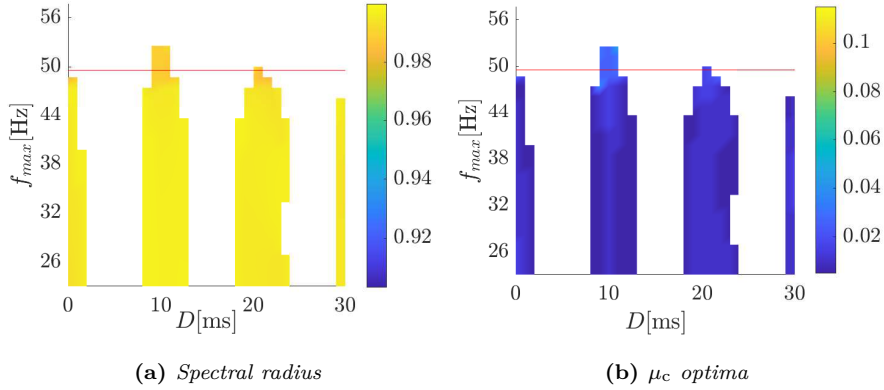
Figure 6: *Stability analysis of the step-by-step updating scheme with contact stiffness* $k_c = 6 \cdot 10^5$ *N/m.*

5. HIL tests results

This section is devoted to the practical implementation of the HIL test and a discussion of the results. A stitched catenary [16] and a simple catenary [17] are modelled by PFEM for the numerical model, since they are the two most representative catenary types. A single span of each catenary model is depicted in Fig. 7. The time step used in all the examples studied is $\Delta t = 2$ ms and the span-by-span updating strategy was selected for stability reasons, as concluded in Section 4. Each HIL test is performed for 120 s, the initial ramp being active in the first 40 s, so that $N_r = 20000$. The relaxation coefficients are $\mu_c = 0.1$ and $\mu_d = 1$. The number of harmonics included in $\mathbf{z}$ and $\mathbf{\Delta L}$, N_h and N_{hd} respectively, are tuned to include the maximum frequency content that provides stable tests. All the results of the experimental HIL tests shown were obtained as the average of 10 spans in which the steady-state response was achieved.

Additional tests are performed to validate the accuracy of the results before the HIL tests on the pantograph.

18
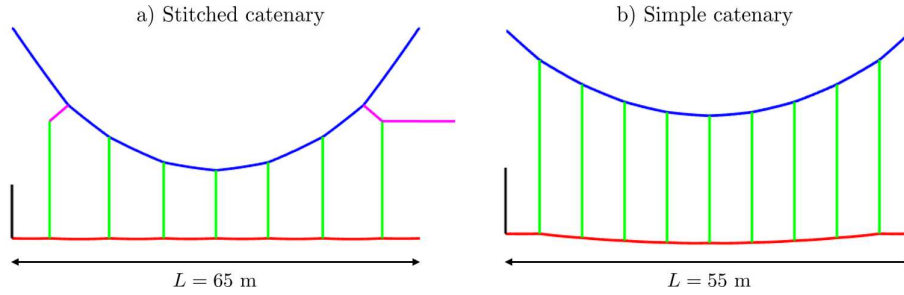
Figure 7: *a) Stitched and b) simple catenary spans for the PFEM catenary models.*

5.1. HIL test validation with an attached mass

To validate the results obtained from the HIL tests, we use the same strategy as that proposed in [18], which consists of attaching an aluminium mass directly to the load cells to take on the role of a hardware device replacing the pantograph. A photo of the assembly described with the attached mass is provided in Fig 8. The whole HIL test can be accurately simulated by computer for this scenario, which avoids the uncertainties of using a mathematical pantograph model. The results of these full HIL simulations can serve as a validation reference for the whole HIL setup (measurement, communication, computation time, delay, etc.).
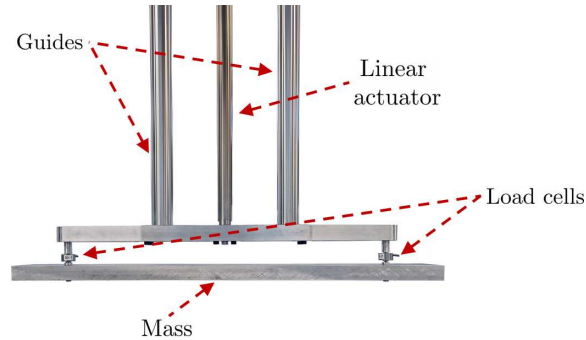
Figure 8: *Aluminium mass acting as hardware substructure for validation purposes.*

The contact force between the mass and the virtual catenary obtained from the HIL test and the simulated HIL are compared in Fig. 9. The forces repre-

19

sented are the mean of the ten last $\mathbf{f}^k$ when the steady state is achieved. In this example, the simulated speed is $v = 250$ km/h (Fig. 9a) and $v = 300$ km/h (Fig. 9b) and the interaction takes place with the stitched catenary (see Fig. 7a). We used $N_{\mathrm{h}} = 25$ for 250 km/h and $N_{\mathrm{h}} = 21$ for 300 km/h to consider frequencies up to 25 Hz in both cases. A delay of $D = 8$ time steps (16 ms) was used to anticipate the reference position. The good agreement between both the experimental and simulated contact forces indicates that the HIL test rig is properly calibrated to provide accurate results.
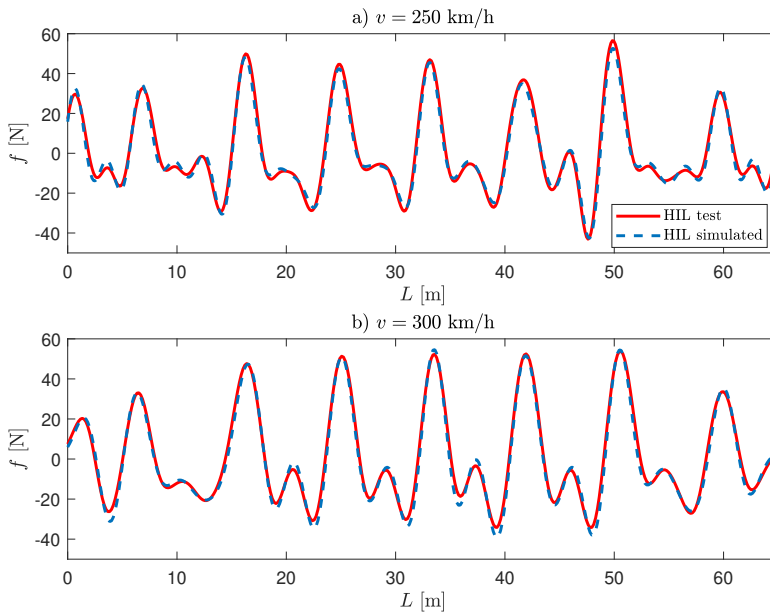
Figure 9: *Comparison of contact forces obtained from experimental HIL tests (solid line) and virtual HIL (dashed line) with the mass travelling at a) 250 km/h and b) 300 km/h.*

In the previous example any dropper could slacken, so that only the linear response of the catenary PFEM was active. To also validate the HIL test setup with nonlinear catenary behaviour, the HIL test with the mass virtually moving at 300 km/h was repeated, but now we added numerically 160 N to the force

20

measured by the load cells. The resulting force was that applied to the virtual catenary. As can be seen in Fig. 10, not only does the contact force measured agree with that obtained from the pure simulated HIL, but the slackened dropper correction forces are also in very good agreement.
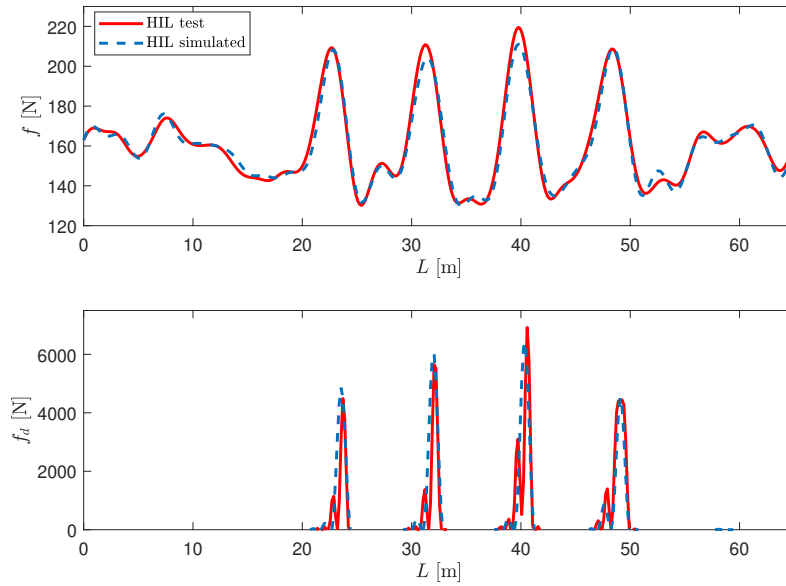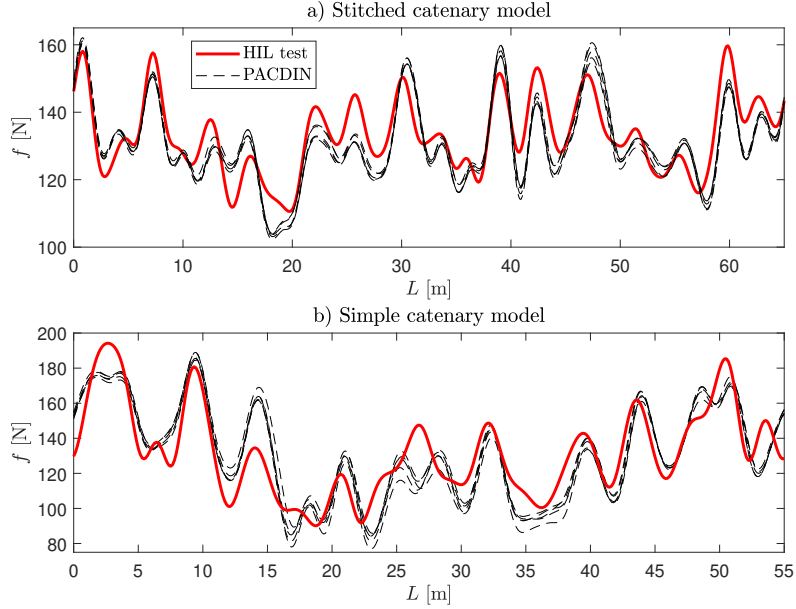

Figure 10: *Comparison of contact forces (top figure) and slackened dropper correction forces (bottom figure) obtained from experimental HIL tests (solid line) and virtual HIL simulations (dashed line) with the mass travelling at 300 km/h and a mean pushing force of 160 N.*

5.2. HIL tests with the pantograph DSA-380

This section gives the results of the HIL tests with the real pantograph DSA-380 interacting with a virtual periodic catenary. As previously mentioned, we use a PFEM of both the stitched and the simple catenaries shown in Fig. 7. The experimental results are compared in this case with the contact force obtained from a standard simulation of the pantograph-catenary dynamic interaction. We use PACDIN software [19] to perform these simulations, which participated in the benchmark exercise [17]. The catenary model simulated in PACDIN has

21

repetitive spans and is long enough to guarantee a stationary response in its central spans to obtain comparable results. The contact force on 5 consecutive central spans is selected to make the comparisons, while the pantograph is simulated by a linear lumped mass model.

Figure 11: *Comparison of contact forces obtained from experimental HIL tests (solid line) and conventional simulation with PACDIN of the pantograph-catenary dynamic interaction (dashed line) with the pantograph running at 250 km/h and interacting with a) the stitched catenary model and b) the simple catenary model.*

⁴⁴⁰ The pantograph-catenary contact force obtained from the HIL tests and PACDIN are compared in Figs. 11 and 12 with the pantograph running at 250 and 300 km/h, respectively, for both the simple and stitched catenaries. Although the HIL tests performed include the number of harmonics shown in Table 1, the contact force used in the comparisons is filtered to 25 Hz. This ⁴⁴⁵ frequency exceeds the 20 Hz that must be considered for validation and comparison purposes in this type of simulations according to the standard [20]. The mean value of the contact force given in Table 1 is related to the train speed

22

required to meet the criterion given in standard [21].

Table 1: *Number of harmonics considered in HIL tests and mean value of contact force.*

	Stitched		Simple		
v [km/h]	N_h	N_hd	N_h	N_hd	Mean force [N]
250	31	107	25	90	≈ 130
300	27	90	22	40	≈ 157

Figs. 11 and 12 show that the contact forces computed on PACDIN for 5
consecutive spans overlap each other, indicating that the steady-state regime
was achieved and this solution is suitable to be compared with the PFEM of
the catenaries used in the HIL tests. The other important conclusion drawn
from these results is the notable similarity between the HIL tests and the stan-
dard simulation. As the HIL set-up was properly validated in Section 5.1, the
discrepancies that can be seen in Figs. 11 and 12 are mainly due to the inability
of the pantograph model used in PACDIN to accurately reproduce the dynamic
behaviour of the real pantograph device because non-linear features such as dry
friction or joint clearances are not accounted for in the model.
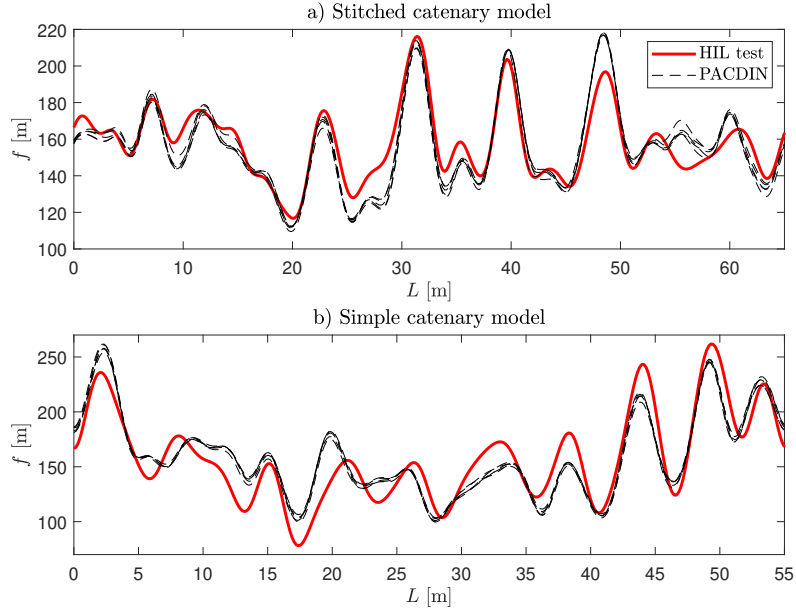
Figure 12: *Comparison of contact forces obtained from experimental HIL tests (solid line) and conventional simulation of the pantograph-catenary dynamic interaction (dashed line) with the pantograph running at 300 km/h and interacting with a) the stitched catenary model and b) the simple catenary model.*
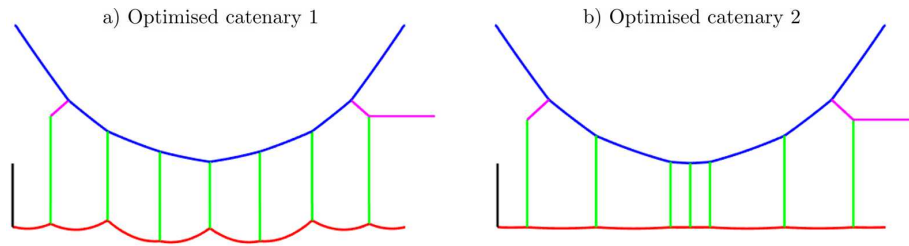
5.3. HIL tests with optimised catenaries

⁴⁶⁰ HIL tests can also be applied to validate the dynamic behaviour of a given catenary model designed or tested only by numerical simulations. TeGreg2018Optim the authors proposed an optimisation of the catenary geometry to obtain the minimum standard deviation of the contact force and therefore to improve the current collection quality when the train travels at 300 km/h. However, the ⁴⁶⁵ optimisation procedure was fully based on numerical simulations in which a lumped mass model of the pantograph was used. To remove the limitations of this simple pantograph model and validate the optimised catenary designs when interacting with a real pantograph, we perform HIL tests in this study using the catenary PFEMs derived from the optimised geometry obtained in ⁴⁷⁰ [16]. The contact wire height at dropper connection points was optimised in the

24

optimised catenary 1 (OC1) and dropper spacing was optimised in optimised catenary 2 (OC2) while keeping the symmetry of the span in both cases. These two optimised geometries can be seen in Fig. 13, in which the vertical scale of OC1 was tuned for a better appreciation of the contact wire height variation along the span.

Figure 13: *PFEM models of optimised stitched catenaries at 300 km/h with a) optimal contact wire height and b) optimal dropper spacing.*

The pantograph-catenary contact force obtained in the HIL tests is plotted in Fig. 14 for both optimised catenaries and is compared with the results of numerical simulations performed with PACDIN, the software used to optimise the catenary geometry [16]. The inputs shown in Table 1 for $v = 300$ km/h are also applied in these HIL tests. The main conclusion of this section is drawn from comparing some statistical parameters of the contact force in the nominal and optimised catenaries. While the former has a maximum contact force of 261.9 N and a minimum contact force of 78 N, these values become 208.2 N and 110 N in the OC1 and, 196.1 N and 124.9 N in the OC2 evidencing a greatly reduction of the maximum value and a considerable increase of the minimum contact force. Furthermore, the contact force standard deviation, which is used as a current collection quality indicator, is 11.24 % and 21.87 % lower for OC1 and OC2 than that obtained from the nominal catenary. These catenary designs therefore still behave better than the nominal design when interacting with a real pantograph, which is a further step towards the final implementation of these optimised overhead contact lines.

25
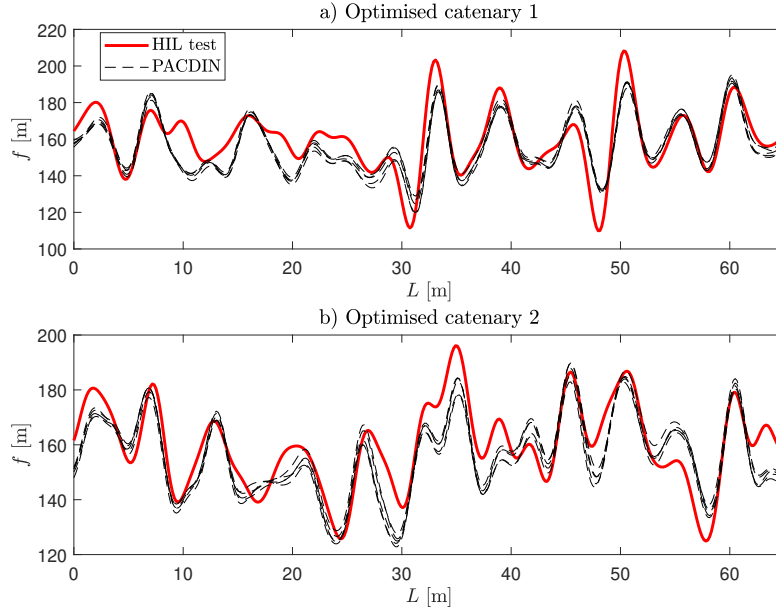
Figure 14: *Comparison of contact forces obtained from experimental HIL tests (solid line) and conventional simulation of the pantograph-catenary dynamic interaction (dashed line) with the pantograph running at 300 km/h and interacting with a) the optimised catenary model 1 and b) the optimised catenary model 2.*

6. Conclusions

The present work addressed the implementation of HIL pantograph tests with the use of a periodic finite element catenary model proposed in [15], although it is limited to the steady-state interaction regime, it incorporates non-linear dropper slackening behaviour and has some important advantages in performing stable HIL tests, such as the ease of tackling delays and limiting the frequency content of the response. Regarding the stability of the iterative scheme used to carry out the HIL tests, a span-by-span updating strategy was proposed and shown to be independent of delay and thus the most robust in practice.

The accuracy of the HIL setup was first validated by a mass block interacting

26

with the virtual catenary with good agreement of the simulation and experimental results. The results of some HIL pantograph tests interacting with different catenaries and travelling at different speeds were then compared with the results of conventional dynamic simulations. The few discrepancies obtained in these comparisons can be attributed to the inability of the linear pantograph model used in the conventional simulations to reproduce the real dynamic pantograph behaviour.

Briefly, the results of the HIL pantograph tests described here offer:

- Accurate spatial discretisation of the catenary by means of the Finite Element Method.

- No boundary effects due to the periodicity condition applied.

- Ideal compensation for the delay.

- Incorporation of dropper slackening behaviour.

However, the proposed approach is limited to the steady-state regime and to considering certain particularities of actual catenaries in HIL tests, factors such as overlapping sections, local irregularities or curved paths are still a matter for further investigation.

Acknowledgements

Appendix A. Formulation for stability analysis

This appendix calculates the terms of Eq. (13) to carry out a virtual HIL simulation in a linear iterative process. The virtual HIL simulation is performed completely in a computational environment in which the pantograph is also

27

simulated. As mentioned in Section 4, this is necessarily an intricate formulation

530 as all the steps carried out for the time integration of a whole span have to be considered in the matrices of Eq. (13). The formulation changes for the two different approaches, the span-by-span and the step-by-step updating strategies.

Appendix A.1. Span-by-span state formulation

For the sake of simplicity and without any loss of generality, let us define the

535 pantograph model as a single degree of freedom model, whose vertical displacement is defined as $y_{\bar{n}}^b$ (for a given span or block b and the time step $\bar{n}$ within this block) and arranged in vector $\mathbf{y}^b$. The state variables chosen for a block b are:

$$\mathbf{X}^b = [\mathbf{z}^{b-2} \quad \mathbf{z}^{b-1} \quad \dot{y}_N^{b-1} \quad y_N^{b-1}]^\top \tag{A.1}$$

which includes the $\mathbf{z}^b$ values of the two previous spans and the displacement

540 and velocity of the pantograph model in the last time step N of the span $b-1$. The state variables for the next span can be computed according to Eq. (13) as:

$$\mathbf{X}^{b+1} = \mathbf{A}\mathbf{X}^b + \mathbf{B} \tag{A.2}$$

To build the matrices $\mathbf{A}$ and $\mathbf{B}$ it is necessary to assemble all the linear operations that happen in the block b. The vertical position $\bar{z}^b(\bar{n})$ or $\bar{z}_{\bar{n}}^b$ of the contact point which will be imposed throughout the block b can be computed

545 from the state vector with Eq. (3). The displacement $\mathbf{y}^b$ of the pantograph model, excited by $\bar{z}_{\bar{n}}^b$, can be obtained using a discrete-time integration scheme. For example, if the Newmark method is chosen, it can be expressed as:

$$\begin{bmatrix} \dot{y} \\ y \end{bmatrix}_{\bar{n}}^b = \hat{\mathbf{A}} \begin{bmatrix} \dot{y} \\ y \end{bmatrix}_{\bar{n}-1}^b + \hat{\mathbf{B}} \, \bar{z}_{\bar{n}-1}^b + \hat{\mathbf{C}} \, \bar{z}_{\bar{n}}^b \tag{A.3}$$

If this iterative scheme is applied recursively from the first time step of the span until a given step $\bar{n}$, it results in:

$$\begin{bmatrix} \dot{y} \\ y \end{bmatrix}_{\bar{n}}^b = \hat{\mathbf{A}}^{\bar{n}} \begin{bmatrix} \dot{y} \\ y \end{bmatrix}_N^{b-1} + \sum_{j=1}^{\bar{n}} \hat{\mathbf{A}}^{\bar{n}-j} \left(\hat{\mathbf{B}} \, \bar{z}_{j-1}^b + \hat{\mathbf{C}} \, \bar{z}_j^b \right) \tag{A.4}$$

28

By rearranging Eq. (A.4), $\mathbf{y}^b$ can be obtained from the linear relation with the state vector:

$$\begin{bmatrix} \dot{\mathbf{y}}^b \\ \mathbf{y}^b \end{bmatrix} = \begin{bmatrix} \mathbf{Q}_1 \\ \mathbf{Q}_2 \end{bmatrix} \mathbf{X}^b \tag{A.5}$$

The measured contact force ($\bar{f}^b(\bar{n})$ arranged in the vector $\bar{\mathbf{f}}^b$) comes from the *penalty* method equation and again, a linear relation can be established:

$$\bar{\mathbf{f}}^b = k_c(\mathbf{y}^b - \bar{\mathbf{z}}^b) \equiv \mathbf{R}\mathbf{X}^b \tag{A.6}$$

As described in the span-by-span updating strategy (see Section 3.3), in point 5 of Fig. 3, the vector $\mathbf{z}^b$ is fully defined when $\bar{n} = N$, time step in which $\mathbf{f}^k = \bar{\mathbf{f}}^b$. Thus, according to Eq. (1):

$$\mathbf{z}^b = \mathbf{z}_0 + \mathbf{I}_{cc}\bar{\mathbf{f}}^b \tag{A.7}$$

Additionally, as the force has not been included in the state vector, the relaxation coefficient can be applied here equivalently:

$$\mathbf{z}^b = \mu_c(\mathbf{z}_0 + \mathbf{I}_{cc}\bar{\mathbf{f}}^b) + (1 - \mu_c)\mathbf{z}^{b-1} \equiv \mathbf{S}\mathbf{X}^b + \mu_c\mathbf{z}_0 \tag{A.8}$$

The state vector of the next span can be built as:

$$\mathbf{X}^{b+1} = [\mathbf{z}^{b-1} \ \ \mathbf{z}^b \ \ \dot{y}_N^b \ \ y_N^b]^\top = [\mathbf{z}^{b-1} \ \ \mathbf{S}\mathbf{X}^b + \mu_c\mathbf{z}_0 \ \ \mathbf{Q}_1|_N\mathbf{X}^b \ \ \mathbf{Q}_2|_N\mathbf{X}^b]^\top \tag{A.9}$$

in which $|_N$ refers to the N row.

So far, the delay has not been considered but its unavoidable existence in a real HIL test affects its stability. The formulation can then be modified to consider a delay of D time steps in the imposed displacement $\bar{z}^b(\bar{n})$, affecting Eq. (3):

$$\bar{z}^b(\bar{n}) = \begin{cases} N_1(m)z^{b-3}(m) + N_2(m)z^{b-2}(m) & \text{if } \bar{n} \leq D \\ N_1(\bar{n}-D)z^{b-2}(\bar{n}-D) + N_2(\bar{n}-D)z^{b-1}(\bar{n}-D) & \text{if } \bar{n} > D \end{cases} \tag{A.10}$$

being $m = N+\bar{n}-D$ and therefore, at least the last D values of $\mathbf{z}^{b-3}$ should be included in the state. As the delay in the HIL test is known, the compensation can be applied by defining $\mathbf{z}^b$ as:

$$\mathbf{z}^b = [z(N-D+1) \ \ z(N-D+2) \ \ ... \ \ z(N) \ \ z(1) \ \ z(2) \ \ ... \ \ z(N-D)]^\top \tag{A.11}$$

29

Appendix A.2. Step-by-step state formulation

The stability of the HIL iterative procedure depends on the updating strat-
egy followed. In this section, we describe the procedure to obtain the iterative
linear operation that applies between consecutive spans for the step-by-step
approach. In this case, the state variables vector includes the displacement im-
posed in the last step of the previous block, the relaxed force of the previous
block and the velocity and displacement of the pantograph model in the last
step of the previous block, respectively. That is:

$$\mathbf{X}^b = [\bar{z}_N^{b-1} \quad {}^{\mathrm{r}}\bar{\mathbf{f}}^{b-1} \quad \dot{y}_N^{b-1} \quad y_N^{b-1}]^\top \tag{A.12}$$

Now the displacement $\bar{\mathbf{z}}^b$ of the contact point imposed comes from Eq. (1),
taken by considering that the vector $\mathbf{f}^k$ is made up of values of the contact force
from both the previous and the current block:

$$\bar{\mathbf{z}}^b = \mathbf{z}_0 + \mathbf{T}\bar{\mathbf{f}}^b + \mathbf{U}^{\mathrm{r}}\bar{\mathbf{f}}^{b-1} \equiv \mathbf{z}_0 + \mathbf{T}\bar{\mathbf{f}}^b + \mathbf{V}\mathbf{X}^b \tag{A.13}$$

in which $\mathbf{T} = \mu_{\mathrm{c}}\mathbf{I}_{\mathrm{cc}}\mathbf{W}$ and $\mathbf{U} = \mathbf{I}_{\mathrm{cc}} - \mathbf{T}$ with:

$$\mathbf{W} = \begin{bmatrix} 0 & 0 & 0 & \cdots \\ 1 & 0 & 0 & \cdots \\ 1 & 1 & 0 & \cdots \\ \vdots & \vdots & \vdots & \ddots \end{bmatrix} \tag{A.14}$$

Eq. (A.4) provides the pantograph model displacement $\mathbf{y}^b$ produced by $\bar{\mathbf{z}}^b$
and this equation can be written as:

$$\mathbf{y}^b = \mathbf{Y}\bar{\mathbf{z}}^b + \mathbf{Z}\mathbf{X}^b \tag{A.15}$$

Eqs. (A.6), (A.13) and (A.15) form a linear system whose unknowns are $\bar{\mathbf{f}}^b$,
$\bar{\mathbf{z}}^b$ and $\mathbf{y}^b$. Once solved, the state variables of the next span can be built as:

$$\mathbf{X}^{b+1} = [\bar{z}_N^b \quad {}^{\mathrm{r}}\bar{\mathbf{f}}^b \quad \dot{y}_N^b \quad y_N^b]^\top \tag{A.16}$$

in which ${}^{\mathrm{r}}\bar{\mathbf{f}}^b = \mu_{\mathrm{c}}\bar{\mathbf{f}}^b + (1-\mu_{\mathrm{c}}){}^{\mathrm{r}}\bar{\mathbf{f}}^{b-1}$. A delay of D time steps and its compensation
can be added to the formulation as in the span-by-span updating strategy.

References

[1] W. Song, C.-M. Chang, V. Dertimanis, Editorial: Recent advances and applications of hybrid simulation, *Frontiers in Built Environment* 6 (2020). doi:10.3389/fbuil.2020.625197.

[2] W. Zhang, G. Mei, X. Wu, Z. Shen, Hybrid simulation of dynamics for the pantograph-catenary system, *Veh. Syst. Dyn.* 38 (6) (2002) 393–414. doi:https://doi.org/10.1076/vesd.38.6.393.8347.

[3] W. Zhang, G. Mei, X. Wu, L. Chen, A study on dynamic behaviour of pantographs by using hybrid simulation method, *Proc. Inst. Mech. Eng. F: J. Rail Rapid Transit* 219 (3) (2005) 189–199. doi:https://doi.org/10.1243/095440905X8880.

[4] S. Gregori, M. Tur, A. Pedrosa, J. Tarancón, F. Fuenmayor, A modal coordinate catenary model for the real-time simulation of the pantograph-catenary dynamic interaction, *Finite Elem. Anal. Des.* 162 (2019) 1–12. doi:10.1016/j.finel.2019.05.001.

[5] A. Collina, A. Facchinetti, F. Fossati, F. Resta, Hardware in the loop test-rig for identification and control application on high speed pantographs, *Shock Vib.* 11 (2004) 445–456. doi:https://doi.org/10.1155/2004/740146.

[6] F. Resta, A. Facchinetti, A. Collina, G. Bucca, On the use of a hardware in the loop set-up for pantograph dynamics evaluation, *Veh. Syst. Dyn,* 46 (S1) (2008) 1039–1052. doi:https://doi.org/10.1080/00423110802037891.

[7] A. Schirrer, G. Aschauer, E. Talic, M. Kozek, S. Jakubek, Catenary emulation for hardware-in-the-loop pantograph testing with a model predictive energy-conserving control algorithm, *Mechatronics* 41 (2017) 17 – 28. doi:https://doi.org/10.1016/j.mechatronics.2016.11.002.

[8] H. Zhou, B. Zhang, X. Shao, Y. Tian, C. Zeng, W. Guo, T. Wang, Recursive predictive optimal control algorithm for real-time hybrid simulation of vehicle–bridge coupling system, *International Journal of Structural Stability and Dynamics* 22 (03 2022). `doi:10.1142/S0219455422410115`.

[9] T. Horiuchi, M. Inoue, T. Konno, Y. Namita, Real-time hybrid experimental system with actuator delay compensation and its application to a piping system with energy absorber, *Earthquake Engineering & Structural Dynamics* 28 (10) (1999) 1121–1141. `doi:https://doi.org/10.1002/(SICI)1096-9845(199910)28:10<1121::AID-EQE858>3.0.CO;2-O`.

[10] C. Chen, J. M. Ricles, Analysis of actuator delay compensation methods for real-time testing, *Engineering Structures* 31 (11) (2009) 2643–2655. `doi:https://doi.org/10.1016/j.engstruct.2009.06.012`.

[11] R.-Y. Jung, P. Benson Shing, E. Stauffer, B. Thoen, Performance of a real-time pseudodynamic test system considering nonlinear structural response, *Earthquake Engineering & Structural Dynamics* 36 (12) (2007) 1785–1809. `doi:https://doi.org/10.1002/eqe.722`.

[12] D. P. Stoten, T. Yamaguchi, Y. Yamashita, Dynamically substructured system testing for railway vehicle pantographs, *Journal of Physics: Conference Series* 744 (2016) 012204. `doi:10.1088/1742-6596/744/1/012204`.

[13] S. Kobayashi, D. P. Stoten, Y. Yamashita, T. Usuda, Dynamically substructured testing of railway pantograph/catenary systems, *Proceedings of the Institution of Mechanical Engineers, Part F: Journal of Rail and Rapid Transit* 233 (5) (2019) 516–525. `doi:10.1177/0954409718799900`.

[14] S. Kobayashi, Y. Yamashita, T. Usuda, D. Stoten, Hybrid simulation testing of a pantograph-catenary system using a dynamically substructured system framework and a mdof catenary model, *Quarterly Report of RTRI* 61 (2020) 127–132. `doi:10.2219/rtriqr.61.2_127`.

[15] J. Gil, M. Tur, S. Gregori, A. Correcher, F. Fuenmayor, Finite element periodic catenary model to perform hil pantograph tests considering non-linear dropper behaviour, *Finite Elements in Analysis and Design* 210 (2022) 103816. `doi:https://doi.org/10.1016/j.finel.2022.103816`.

[16] S. Gregori, M. Tur, E. Nadal, F. J. Fuenmayor, An approach to geometric optimisation of railway catenaries, *Vehicle System Dynamics* 56 (8) (2018) 1162–1186. `doi:https://doi.org/10.1080/00423114.2017.1407434`.

[17] S. Bruni, J. Ambrosio, A. Carnicero, Y. H. Cho, L. Finner, M. Ikeda, S. Y. Kwon, J. P. Massat, S. Stichel, M. Tur, The results of the pantograph-catenary interaction benchmark, *Veh Syst. Dyn.* 53 (3) (2015) 412–435. `doi:https://doi.org/10.1080/00423114.2014.953183`.

[18] J. Gil, M. Tur, A. Correcher, S. Gregori, A. Pedrosa, F. J. Fuenmayor, Hardware-in-the-loop pantograph tests using analytical catenary models, *Veh Syst. Dyn.* 60 (10) (2022) 3504–3518. `doi:https://doi.org/10.1080/00423114.2021.1962538`.

[19] M. Tur, L. Baeza, F. Fuenmayor, E. García, PACDIN statement of methods, *Vehicle System Dynamics* 53 (3) (2015) 402–411. `doi:https://doi.org/10.1080/00423114.2014.963126`.

[20] EN 50318:2018, Railway applications. Current collection systems. Validation of simulation of the dynamic interaction between pantograph and overhead contact line, *European Committee for Electrotechnical Standardization (CENELEC)* (2018).

[21] EN 50367:2012, Railway applications. Current collection systems. Technical criteria for the interaction between pantograph and overhead line, *European Committee for Electrotechnical Standardization (CENELEC)* (2012).